Graphene Microcapsule Arrays for Combinatorial Electron Microscopy and Spectroscopy in Liquids

Alexander Yulaev[1,2,3], Hongxuan Guo[1,3], Evgheni Strelcov[1,3], Lei Chen[1], Ivan Vlassiouk[4], and Andrei Kolmakov[1]*

[1]Center for Nanoscale Science and Technology, NIST, Gaithersburg, MD 20899, USA

[2]Department of Materials Science and Engineering, University of Maryland, College Park, MD 20742, USA;

[3]Maryland NanoCenter, University of Maryland, College Park, MD 20742, USA;

[4]Oak Ridge National Laboratory, Oak Ridge, TN 37831, USA;

*Corresponding author: andrei.kolmakov@nist.gov

Gray scale value analysis of SEM contrast of liquid, vapor, empty with continuous Gr, and empty with broken Gr membrane channels
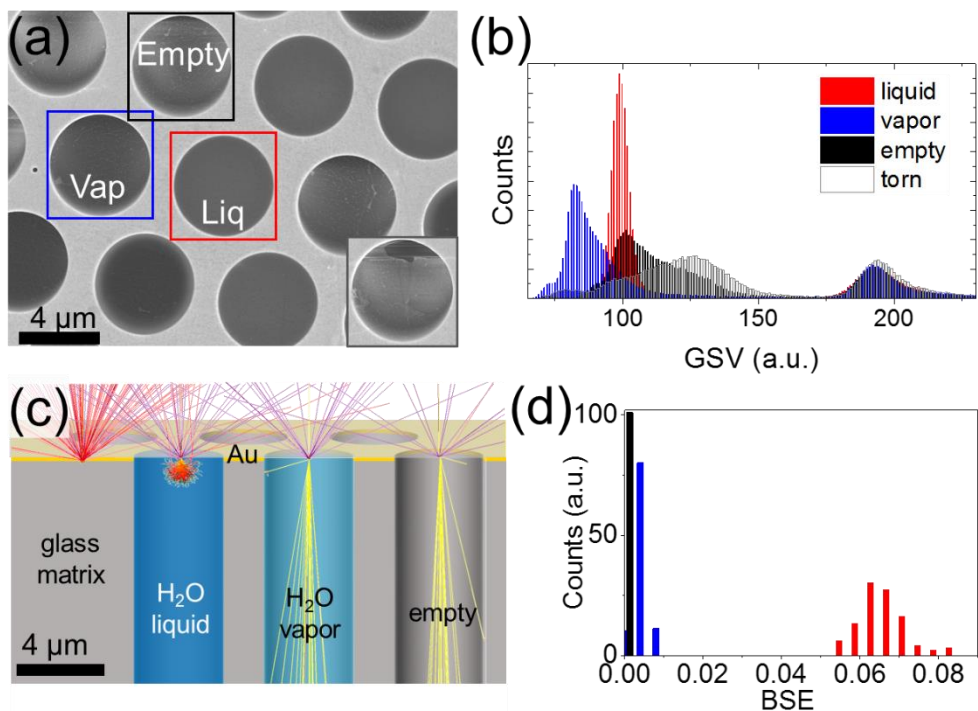

Figure S1. Gray scale value analysis of MCA channels of different types. (a) SEM image (E_{beam}=10 keV) of empty, water-filled, vapor-filled, and broken MCA channels; all sealed with a bilayer graphene. Bright (framed with black square), uniformly gray (framed with red square), uniformly dark (framed with blue square), and with a tear (framed with gray square) channels corresponding to empty, water, vapor filled channels, and a broken one, respectively. (b) The color coded histogram showing the distinctly different distributions of the gray scale values (GSV) inside the corresponding square frames. (c) Monte-Carlo trajectories simulations of 8 keV electron beam interacting with an empty (vacuum-filled) channel, a water-vapor-filled channel (assuming 3.17 kPa saturated vapor pressure at 25 ˚C), a liquid-water-filled channel, and the gold MCA surface. The number of BSEs is proportional to the density and Z-number of the sample, and varies inversely with the probing depth. (c) The BSE coefficients from 100 Monte-Carlo simulations for empty (black), vapor filled (blue), and water filled (red) channels
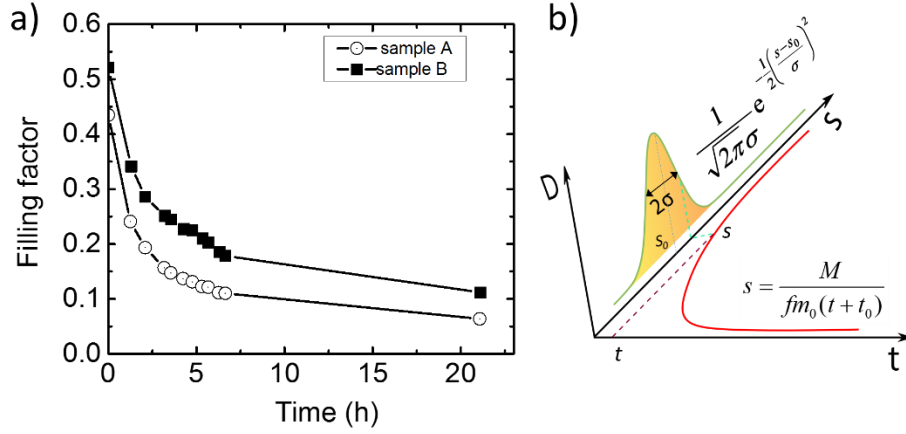
Liquid water retention time inside MCA in a vacuum

Figure S2. Water retention lifetime measurement of an MCA in a vacuum environment. (a) Experimental temporal evolution of the filling factor (i.e. ratio of filled channels to all MCA channels) for two randomly selected MCA samples. (b) An illustration of the model for liquid lifetime assessment in MCA. The yellow area demonstrates the normal distribution of defects in graphene with a total effective area s, for an individual graphene cupped channel. Here s_0 and σ are the mean value and standard deviation respectively. The red curve depicts the relation between s and water retention lifetime t for MCA in a vacuum based on assumption of Knudsen effusion. Here M is the initial water mass inside the individual channel, f is a Knudsen flux per unit areas (see text) and m_0 is the water molecular mass

To estimate the water retention time inside MCA in a vacuum, we assumed a normal distribution of effective area s of defects in every graphene-capped 5 µm wide MCA channel. At the defective sites, water effusion can be described with Knudsen's equation for a molecular flux per unit area:

$$f = \frac{P_{\mathrm{S}}}{\sqrt{2\pi m_0 kT}},$$ (1)

where P_{S} is the saturated water pressure at room temperature, m_0 is the mass of a water molecule, T is room temperature, and k is Boltzmann constant. The normal distribution of graphene defects, s, is expressed by

$$D(s) = A \frac{1}{\sqrt{2\pi}\sigma} \mathrm{e}^{\frac{(s-s_0)^2}{2\sigma^2}},$$ (2)

where σ and s_0 stand for the standard deviation and mean area of defects, respectively. A is a constant to normalize the distribution between $s = 0$ (channels without leak) and the maximal opening $s = S$ (channels without membrane). Each filled channel has to lose a fixed amount of

water of mass *M* to become empty. To obtain the temporal dependence of the filling factor, we integrate the normal distribution within 0 to t domain. After integration and normalization, the filling factor is:

$$Y(t) = \frac{erf\left(\dfrac{\dfrac{M}{fm_0}\dfrac{1}{t+t_0} - s_0}{\sqrt{2}\sigma}\right) - erf\left(\dfrac{-s_0}{\sqrt{2}\sigma}\right)}{erf\left(\dfrac{S-s_0}{\sqrt{2}\sigma}\right) - erf\left(\dfrac{-s_0}{\sqrt{2}\sigma}\right)}, \tag{3}$$

where t_0 is the moment when water starts evaporating. The latter was used to fit experimental data in the figure 2e of the main text.

Liquid water contrast in SEM

An electric potential on Everhart-Thornley (E-T) detector with a positively biased Faraday cage was set to collect secondary electrons (SE). Under these settings, most of the SEs and a fraction of back scattered electrons (BSE) were collected. The gray scale values of the SEM images are, therefore, proportional to the local total electron yield detected. When the primary electron beam hits an MCA channel without graphene, (or capped with broken one) it inevitably charges the inner glass walls of the high aspect ratio microchannel. The accumulating charge causes an increase of the SE electron signal and explains the elevated gray scale values from those channels. Similar scattering and charging take place inside the empty microchannels that are completely covered with a double layer graphene membrane. Gray scale values for those channels are lower compared to ones with broken (missing) graphene due to attenuation of the SEs and BSEs by the graphene membrane. Due to inhomogeneous charging, none of these groups of channels were used for image analysis. Different from the above, channels filled with water vapor do not exhibit charging of their walls. Since the intensity of BSE and SE generated by the vapor is very small, only SE_m and BSE_m from the graphene membrane can be detected by the SEM detector. This is why vapor filled channels exhibit the lowest secondary electron signal

$$S_{\text{vapor}} \approx SE_m + BSE_m. \tag{4}$$

When the channel is filled with water, the SEM signal from water cell capped with graphene S_{water} includes:

$$S_{\text{water}} = SE_m + BSE_m + \eta_{SE}SE_{\text{water}} + \eta_{BSE}BSE_{\text{water}} + SE_{\text{water}-m}; \tag{5}$$

Where $SE_{\text{water-m}}$ is the secondary electrons generated inside the graphene membrane by outgoing BSE emitted in water and η is an energy dependent attenuation factor accounting for attenuation of the electron flux by the graphene membrane. It is convenient to use SEM signal from the gold coated MCA as a reference. Similar to (5), SEM signal from the graphene coated Au film can be written as

$$S_{\text{Au}} = SE_{\text{m}} + BSE_{\text{m}} + \eta_{\text{SE}}SE_{\text{Au}} + \eta_{\text{BSE}}BSE_{\text{Au}} + SE_{\text{Au-m}}. \tag{6}$$

Here, SE_{Au-m} is the intensity of the secondary electrons generated in graphene by BSE scattered in Au film. Now we can introduce a relative contrast value:

$$\beta = \frac{S_{\text{water}} - S_{\text{vapor}}}{S_{\text{Au}} - S_{\text{vapor}}} = \frac{\eta_{\text{SE}}SE_{\text{water}} + \eta_{\text{BSE}}BSE_{\text{water}} + SE_{\text{water-m}}}{\eta_{\text{SE}}SE_{\text{Au}} + \eta_{\text{BSE}}BSE_{\text{Au}} + SE_{\text{Au-m}}}. \tag{7}$$

The dependence of β on electron beam energy is shown in the Figure 2 c of the main text and in the Figure S3. If an electron attenuation length is significantly larger than graphene membrane thickness, we can neglect the $SE_{water-m}$ and SE_{Au-m} terms. Thus, we obtain:

$$\beta = \frac{\sigma_{\text{water}}}{\sigma_{\text{Au}}}. \tag{8}$$

Here, σ_{water} and σ_{Au} are the total electron yields of water and gold, respectively (both values depend on the primary beam energy).
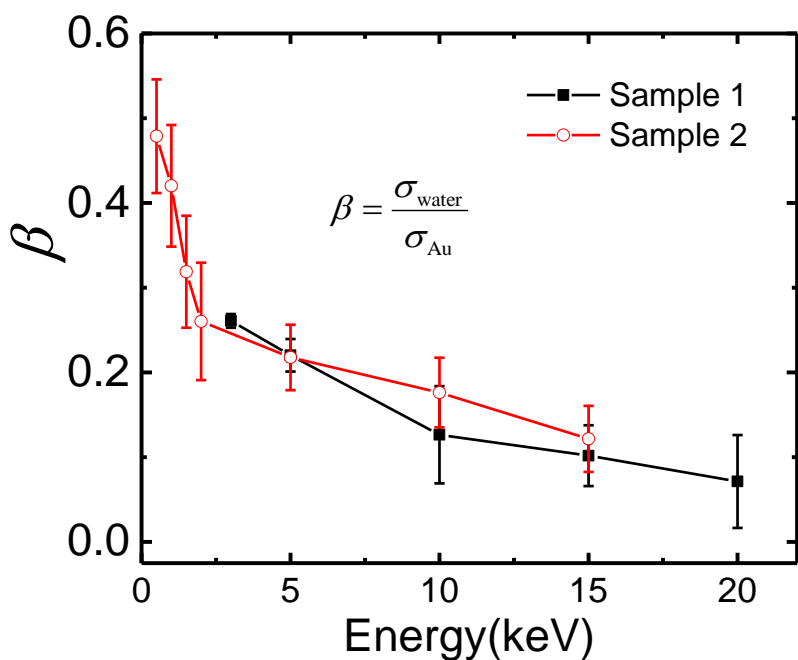
Figure S3. Ratio of electron intensity from water and Au vs. incident beam energy measured for two MCA samples. Error bars show the variation of results from different area.

This condition occurs at high electron beam energy and, since the SE/BSE ratio generally decreases with energy[1], β approaches the ratio of the corresponding BSE coefficients. Conversely, at low electron energy the surface sensitive secondary electrons and corresponding attenuation factors contribute majorly to β parameter and, therefore, it approaches 1 when the graphene membrane dominates the signal independently on the region of interest.
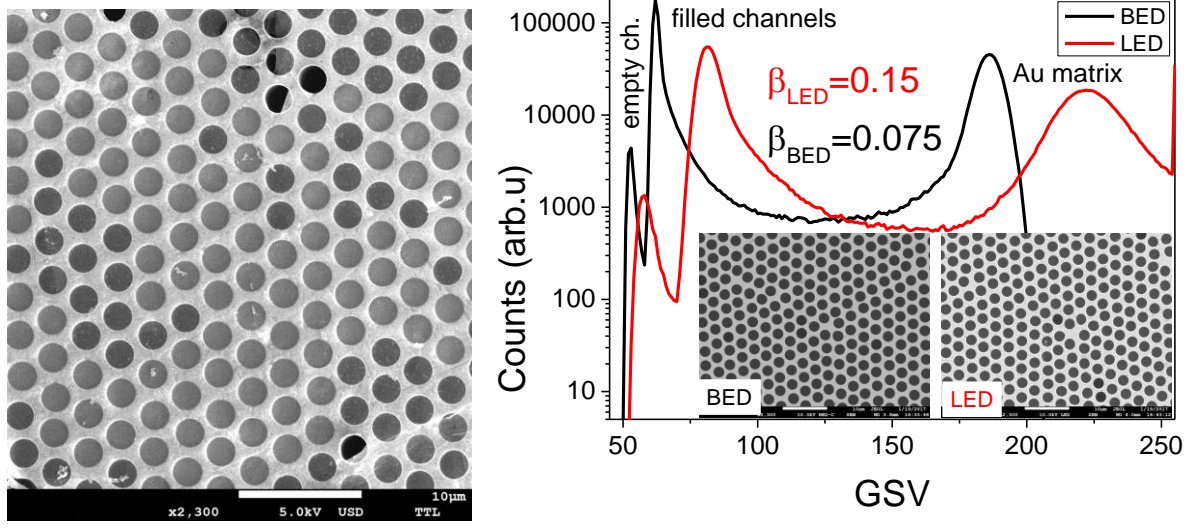
Figure S3a. Left: a TTL secondary electron image of water-filled MCA (E_{beam}=5 keV); Right: SEM gray scale values (GSV) histograms of water-filled MCA recorded simultaneously from the same area (insets) using standard ET (LED) and BED SEM detectors (E_{beam}=10 keV)

Due to high secondary electron contribution form liquid layers below graphene the employment of the through-the-lens (TTL) or E-T type lower electron detectors (LED) is preferable over back scattered electrons detector (BED) in a wide energy range of primary electrons. As an example, water filled channels can be easily discriminated from the empty ones in the Fig. S2a (left panel). In practice, even for 10 keV primary electron beam the β-parameter measured with LED is twice larger compared to one recorded using BED (Fig.2a, right panel). This is due to significant contribution of the $\eta_{SE}SE_{water}$ partition (see eq. 7) to the total electron signal measured by LED.

AES in water

A water channel covered with graphene was characterized by Auger spectroscopy. Figures 3a and 3e of the main text show the geometry of the experiments and typical C_{KLL} and O_{KLL} differential AES spectra in the graphene capped empty and water filled channels. Using standard attenuation formula,[2] the intensity of the C_{KLL} peak of graphene with an effective thickness δ_G can be calculated as:

$$I_{C_{KLL}} = I_0 \sigma_{C_{KLL}} \gamma_{C_{KLL}} F(E_{C_{KLL}}) D(E_{C_{KLL}}) N_G [1 + r(E_0, \alpha)] \int_0^{\delta_G} e^{\frac{-z}{\lambda_{C-G} \sin\theta}} dz \,,$$

Similarly, the intensity of the water O_{KLL} peak attenuated by the graphene membrane cap can be written as[2]:

$$I_{\text{O}_{\text{KLL}}} = I_0 \sigma_{\text{O}_{\text{KLL}}} \gamma_{\text{O}_{\text{KLL}}} F(E_{\text{O}_{\text{KLL}}}) D(E_{\text{O}_{\text{KLL}}}) N_{\text{W}} [1 + r(E_0, \alpha)] e^{\frac{-\delta_{\text{G}}}{\lambda_{\text{O-G}} \sin\theta}} \int_0^{\delta_{\text{W}}} e^{\frac{-z}{\lambda_{\text{O-w}} \sin\theta}} dz \ ,$$

Where I_0 is the intensity of the primary electron beam, $\sigma_{\text{C}_{\text{KLL}}}$ and $\sigma_{\text{O}_{\text{KLL}}}$ are the K shell ionization cross sections of C and O for primary electrons with energy of E_0, which are $1.95 \times 10^{-19} \text{cm}^2$ and $0.82 \times 10^{-19} \text{cm}^2$, respectively.[3] $\gamma_{\text{C}_{\text{KLL}}}$ and $\gamma_{\text{O}_{\text{KLL}}}$ are the probabilities that the ionized core level K in elements C and O will emit KLL Auger electrons, which are 0.9988 and 0.9963, respectively.[4] $D(E_{\text{C}_{\text{KLL}}})$ and $D(E_{\text{O}_{\text{KLL}}})$ are the collection efficiency of detector, which is assumed to be constant for all Auger electrons with energies above 200 eV.[5] $F(E_{\text{C}_{\text{KLL}}})$ and $F(E_{\text{O}_{\text{KLL}}})$ are the transmission efficiency of the electron spectrometer to be proportional to corresponding Auger electron energies when the spectrometer was operated in a constant retarding ratio mode.[6] N_{G} and N_{W} are the atomic densities of the graphene $113 \, \text{nm}^{-3}$ and water $33.4 \, \text{nm}^{-3}$, respectively. $r(E_0, \alpha) = 0.255$ is Monte Carlo simulated backscattering-correction-factor[7] for 5 kV primary electrons propagating in water. λ_{CG}, λ_{OG}, and λ_{OW} are the attenuation lengths of the C_{KLL} Auger electrons in graphene, the O_{KLL} Auger electrons in graphene, the O_{KLL} Auger electrons in water, respectively. We used $\lambda_{\text{CG}} = 0.65 \, \text{nm}$ and $\lambda_{\text{OG}} = 1.29 \, \text{nm}$ from previous AES data[8]. For λ_{OW} we used 3.1 nm as measured by liquid micro-jet photoelectron spectroscopy.[9] The ratio between the C_{KLL} and O_{KLL} peak intensities for a T_{G} thick graphene membrane capping a T_{W} thick water layer can be calculated using the sample structure (Figure 3a):

$$\frac{I_{\text{O}_{\text{KLL}}}}{I_{\text{C}_{\text{KLL}}}} = \frac{\sigma_{\text{O}_{\text{KLL}}} \gamma_{\text{O}_{\text{KLL}}} N_{\text{G}} F(E_{\text{O}_{\text{KLL}}})}{\sigma_{\text{C}_{\text{KLL}}} \gamma_{\text{C}_{\text{KLL}}} N_{\text{W}} F(E_{\text{C}_{\text{KLL}}})} \frac{\lambda_{\text{O-W}}}{\lambda_{\text{C-G}}} \frac{1 - e^{-\delta_{\text{W}}/(\lambda_{\text{O-W}} \sin\theta)}}{1 - e^{-\delta_{\text{G}}/(\lambda_{\text{C-G}} \sin\theta)}} e^{-\delta_{\text{G}}/(\lambda_{\text{O-G}} \sin\theta)} \ .$$

For bulk water $\delta_{\text{W}} = \infty$, thus the ratio is reduced to:

$$\frac{I_{\text{O}_{\text{KLL}}}}{I_{\text{C}_{\text{KLL}}}} = \frac{\sigma_{\text{O}_{\text{KLL}}} \gamma_{\text{O}_{\text{KLL}}} N_{\text{G}} F(E_{\text{O}_{\text{KLL}}})}{\sigma_{\text{C}_{\text{KLL}}} \gamma_{\text{C}_{\text{KLL}}} N_{\text{W}} F(E_{\text{C}_{\text{KLL}}})} \frac{\lambda_{\text{OW}}}{\lambda_{\text{CG}}} \frac{1}{1 - e^{-\delta_{\text{G}}/(\lambda_{\text{CG}} \sin\theta)}} e^{-\delta_{\text{G}}/(\lambda_{\text{OG}} \sin\theta)} \ ,$$

In this work, we used the peak-to-peak AES intensity ratio instead of area of AES peaks for estimation.
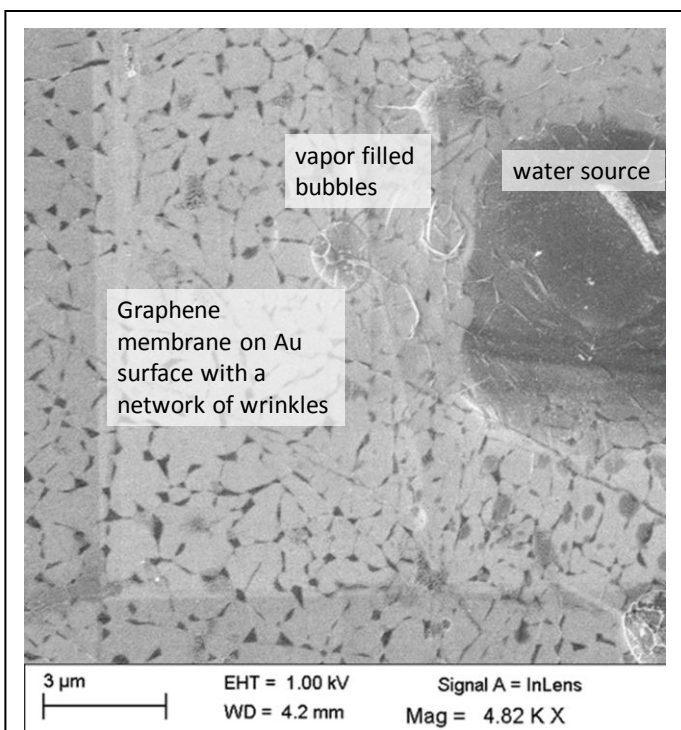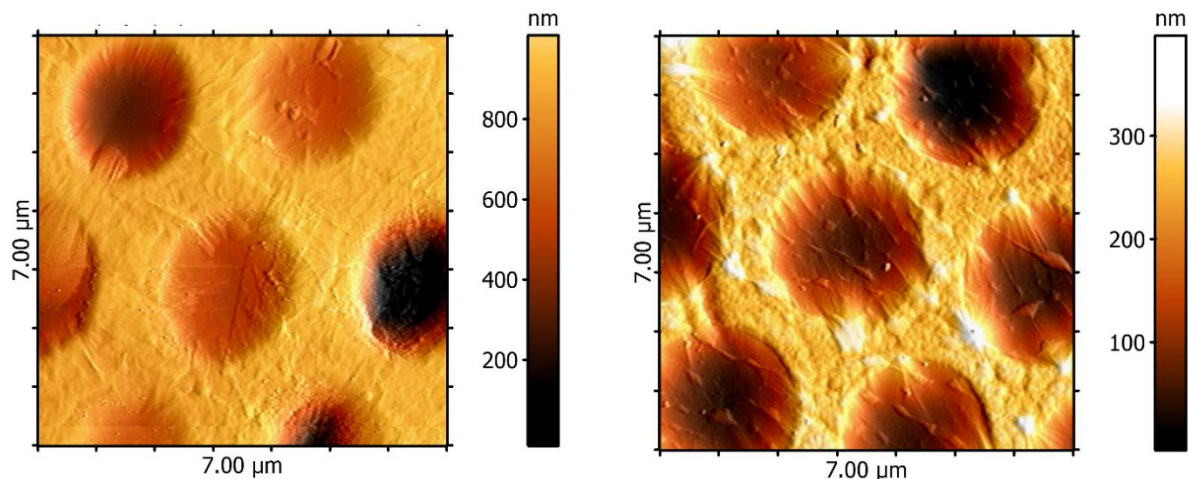
Graphene wrinkles as water diffusion channels

Figure S4a (top). AFM topographic images of bilayer graphene-capped MCA's filled with a 1M $CuSO_4$ electrolyte solution displaying multiple wrinkles and other topographic defects due to non-ideal conformity of the graphene membrane.

Figure S4b (left). Low voltage SEM image of the "under carpet" water diffusion through a network of single layer graphene wrinkles. Unlike vapor-filled bubbles, the water filled-wrinkles appear as dark web-like network due to attenuation of low energy SE from the Au substrate by tens of nm thick water-filled pockets.

TEM graphene characterization

The graphene quality, purity and the number of the graphene layers were assessed in ref.[10], as well as by using HRTEM imaging and fast Fourier transform analysis (Fig.S4). The microscope operated at a primary electron energy of 80 keV. The microscope was equipped with an imaging corrector which yields and 0.7 Å spatial resolution.
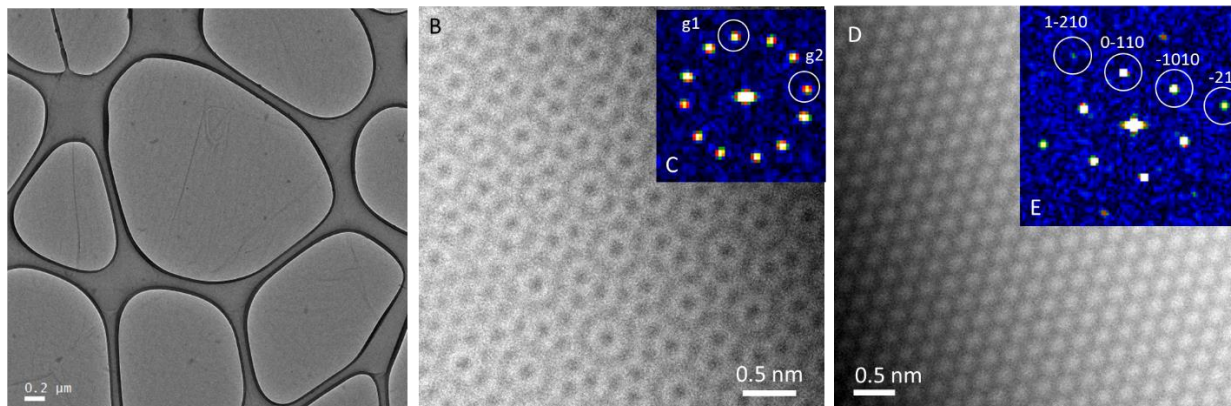
Figure S5. (a) TEM image of bi-layer graphene; (b) Atomic resolution image of bi-layer graphene. (c) A diffractogram of panel a. A total of two sets of six-fold symmetry patterns show the existence of bilayer graphene. (d) for comparison: atomic resolution image of a single layer graphene. €: A diffractogram of panel d. The peak intensity ratio of 0-110 arb. u. and 1-210 arb. u. is higher than one, which confirms that the layer number of the graphene is 1.

In electron diffraction, the ratio of the intensity of the {1100} to {2110} diffraction peaks was used to identify the monolayer graphene. Both computational[11] and experimental studies[12-13] have shown that this ratio is greater than one for monolayer graphene, and less than one for multilayer graphene. The typical six-fold symmetry patterns expected for graphene were used to identify the total number of these monolayer graphene sheets.

More examples of the combinatorial SEM using graphene capped MCA platform
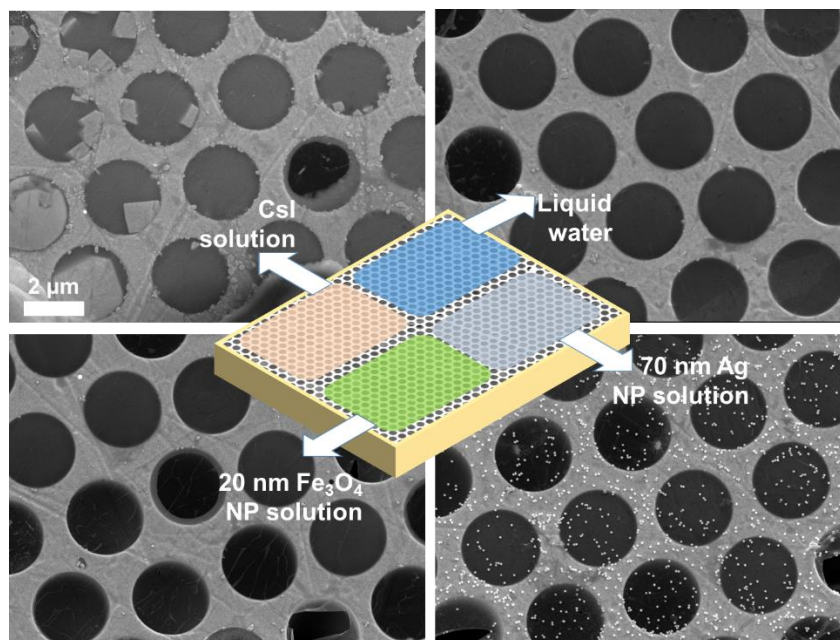

Figure S6. An example of the combinatorial SEM imaging ($E_{beam} = 5$ keV). The quadrants of the bilayer graphene MCA sample were filled with different solutions and imaged with E-T detector under the same contrast brightness settings.

Similar to the bioassay approach, the platform enables combinatorial/comparative SEM analysis of different liquid analytes (Figure S6).

ALD parameters for Pt counter electrode deposition

The MCA plate was placed on a polished Si carrier wafer. The bottom side of the MCA plate therefore was isolated from the precursors. ALD deposition of 10 nm Al_2O_3 film was first initiated to create an adhesion layer via exposing the MCA sample to trimethyl aluminum (TMA) for 20 ms and H_2O for 40 ms at 300 C. Then, 40 nm Pt film was deposited by exposing the MCA samples to trimethyl (methylcyclopentadienyl)-platinum(IV) (MeCpPtMe$_3$) for 1 s at 300 C and 80 mTorr chamber pressure, and O_2 for 50 s at 300 C and 230 mTorr chamber pressure. An idle time of 1 min 20 s is set after MeCpPtMe$_3$ injection to allow the precursor to fill the microchannels with such a high aspect ratio (see also refs.[14-15]) Using these parameters, up to 0.5 of the length of the micro channels can be covered with Pt. After ALD 200 nm/10 nm Au/Cr film was deposited on the opposite face by plasma sputtering.

Sample preparation details

As-grown CVD graphene on copper foil was transferred onto one side of commercially available glass multichannel arrays using PMMA as a sacrificial layer. Briefly, a 200 nm PMMA film was spin-coated onto a graphene/Cu stack followed by etching copper in ammonium persulfate solution (APS) at 40 °C for 2 h. Then, the graphene monolayer was rinsed three times in deionized (DI) water by using wire loop and three 100 mL volumes of DI water. The first graphene was then transferred onto another graphene/Cu foil. After annealing the sample on a hot plate for 2 h at 180 °C, etching in APS and rinsing in DI water were repeated. A PMMA/bilayer graphene stack was transferred onto Au coated MCA face by scooping up the graphene/PMMA stack from water. The sample was annealed on the hot plate for 2 h at 180 °C again. After the graphene transfer, the PMMA was dissolved in acetone bath at 70 °C for ca 20 min. Figure S7 shows typical Raman spectra of suspended membrane on MCA collected at few locations.
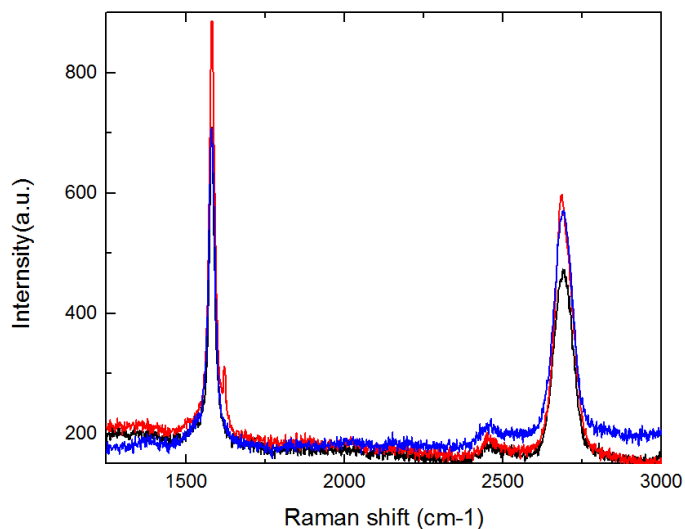
Figure S7 Raman spectra of dry suspended bilayer graphene membrane on MCA collected at few locations

Then, the acetone was gradually substituted with the IPA solution at 80 °C and then with DI water using plastic wash bottles. The latter procedure has to be repeated at least three times and with large amount of water sufficient to   dilute IPA to a negligible level. One should wait ca 10 min between dilution steps to ensure the compositional equilibration inside the channels.

For pure water studies, the sample was removed from the bath and excess of the liquid was carefully removed from the holding tweezers tips and the back side of the MCA using the filter paper strips.

For studies involving electrolytes, a droplet of the electrolyte with known concentration was drop-casted onto the backside of the water filled MCA. The volume of the droplet significantly exceeds the amount of water inside the MCA. After few minutes required for establishing concentration equilibrium, the excess of the droplet was removed with a filter paper by touching the peripheral side of the MCA.

UV curable adhesive or liquid metal such as galinstan was applied about one minute after drying of thin wetting liquid layer at the back side of MCA.

For combinatorial samples the backside of the sample was pre-patterned with strips of a hydrophobic layer before the liquid filling using fine paint brush. This prevented cross-contamination between the analytes during application.

References

1.   Goldstein, J.; Newbury, D.; Joy, D.; Lyman, C.; Echlin, P.; Lifshin, E.; Sawyer, L.; Michael, J.,

Scanning Electron Microscopy and X-ray Microanalysis. **2003**.

2.   Seah, M. P., *Practical Surface Analysis by Auger and X-ray Photoelectron Spectroscopy*. John

Wiley & Sons Ltd.: **1983**; Vol. 189.

3.   Llovet, X.; Powell, C. J.; Salvat, F.; Jablonski, A., Cross Sections for Inner-Shell Ionization by

Electron Impact. *J. Phys. Chem. Ref. Data* **2014,** *43* (1), 013102.

4.   Seah, M. P.; Gilmore, I. S., Quantitative AES. VIII: Analysis of Auger electron intensities from

elemental data in a digital Auger database. *Surf. Interface Anal.* **1998,** *26* (12), 908-929.

5.   Mroczkowski, S.; Lichtman, D., Calculated Auger yields and sensitivity factors for KLL–NOO

transitions with 1–10 kV primary beams. *J Vac Sci Technol A* **1985,** *3* (4), 1860-1865.

6.   Ruffieux, P.; Schwaller, P.; Gröning, O.; Schlapbach, L.; Gröning, P.; Herd, Q.; Funnemann, D.;

Westermann, J., Experimental determination of the transmission factor for the Omicron EA125 electron

analyzer. *Review of Scientific Instruments* **2000,** *71* (10), 3634-3639.

7.   Jablonski, A.; Powell, C. J., *NIST Backscattering-Correction-Factor Database for Auger Electron

Spectroscopy*. National Institute of Standards and Technology: Gaithersburg, Maryland, **2015**.

8.   Xu, M.; Fujita, D.; Gao, J.; Hanagata, N., Auger electron spectroscopy: a rational method for

determining thickness of graphene films. *Acs Nano* **2010,** *4* (5), 2937-2945.

9.   Thürmer, S.; Seidel, R.; Faubel, M.; Eberhardt, W.; Hemminger, J. C.; Bradforth, S. E.; Winter, B.,

Photoelectron Angular Distributions from Liquid Water: Effects of Electron Scattering. *Phys. Rev. Lett.*

2013, *111* (17), 173005.

10.   Yulaev, A.; Cheng, G.; Walker, A. R. H.; Vlassiouk, I. V.; Myers, A.; Leite, M. S.; Kolmakov, A.,

Toward clean suspended CVD graphene. *RSC advances* **2016,** *6* (87), 83954-83962.

11.   Horiuchi, S.; Gotou, T.; Fujiwara, M.; Sotoaka, R.; Hirata, M.; Kimoto, K.; Asaka, T.; Yokosawa, T.; Matsui, Y.; Watanabe, K., Carbon nanofilm with a new structure and property. *Japanese journal of applied physics* **2003,** *42* (9A), L1073.

12.   Hernandez, Y.; Nicolosi, V.; Lotya, M.; Blighe, F. M.; Sun, Z.; De, S.; McGovern, I.; Holland, B.; Byrne, M.; Gun'Ko, Y. K., High-yield production of graphene by liquid-phase exfoliation of graphite. *Nature nanotechnology* **2008,** *3* (9), 563-568.

13.   Wang, C.; Qiao, Q.; Shokuhfar, T.; Klie, R. F., High‐Resolution Electron Microscopy and Spectroscopy of Ferritin in Biocompatible Graphene Liquid Cells and Graphene Sandwiches. *Adv. Mater.* **2014,** *26* (21), 3410-3414.

14.   Miao, H.; Gomella, A. A.; Chedid, N.; Chen, L.; Wen, H., Fabrication of 200 nm period hard X-ray phase gratings. *Nano letters* **2014,** *14* (6), 3453.

15.   Vaish, A.; Krueger, S.; Dimitriou, M.; Majkrzak, C.; Vanderah, D. J.; Chen, L.; Gawrisch, K., Enhancing the platinum atomic layer deposition infiltration depth inside anodic alumina nanoporous membrane. *Journal of Vacuum Science & Technology A: Vacuum, Surfaces, and Films* **2015,** *33* (1), 01A148.